

JGR Space Physics

RESEARCH ARTICLE

10.1029/2020JA027822

Key Points:

- We show two observation events of magnetic reconnection in foreshock transients with and without a strong guide field, respectively
- We identified a super-ion-Alfvénic electron outflow, positive $\mathbf{j} \cdot \mathbf{E}$, and the electron temperature increases without strong ion coupling
- Observation results are qualitatively consistent with particle-in-cell simulation results

Supporting Information:

- Supporting Information S1

Correspondence to:

T. Z. Liu and S. Lu,
terryliuzixu@ucla.edu;
slu@igpp.ucla.edu

Citation:


Liu, T. Z., Lu, S., Turner, D. L., Gingell, I., Angelopoulos, V., Zhang, H., et al. (2020). Magnetospheric Multiscale (MMS) observations of magnetic reconnection in foreshock transients. *Journal of Geophysical Research: Space Physics*, 125, e2020JA027822. <https://doi.org/10.1029/2020JA027822>

Received 15 JAN 2020

Accepted 29 MAR 2020

Accepted article online 4 APR 2020

Magnetospheric Multiscale (MMS) Observations of Magnetic Reconnection in Foreshock Transients

Terry Z. Liu^{1,2} , San Lu³ , Drew L. Turner⁴ , Imogen Gingell⁵, Vassilis Angelopoulos³ , Hui Zhang² , Anton Artemyev³ , and James L. Burch⁶ 

¹Cooperative Programs for the Advancement of Earth System Science, University Corporation for Atmospheric Research, Boulder, CO, USA, ²Geophysical Institute, University of Alaska, Fairbanks, Fairbanks, AK, USA, ³Department of Earth, Planetary, and Space Sciences, University of California, Los Angeles, CA, USA, ⁴Johns Hopkins University Applied Physics Laboratory, Laurel, MD, USA, ⁵School of Physics and Astronomy, University of Southampton, Southampton, UK, ⁶Southwest Research Institute, San Antonio, TX, USA

Abstract Magnetic reconnection is a fundamental process of energy conversion in plasmas between electromagnetic fields and particles. Magnetic reconnection has been observed directly in a variety of plasmas in the solar wind and Earth's magnetosphere. Most recently, electron magnetic reconnection without ion coupling was observed for the first time in the turbulent magnetosheath and within the transition region of Earth's bow shock. In the ion foreshock upstream of Earth's bow shock, there may also be magnetic reconnection especially around foreshock transients that are very turbulent and dynamic. With observations from the National Aeronautics and Space Administration's Magnetospheric Multiscale mission inside foreshock transients, we report two events of magnetic reconnection with and without a strong guide field, respectively. In both events, a super-ion-Alfvénic electron jet was observed within a current sheet with thickness less than or comparable to one ion inertial length. In both events, energy was converted from the magnetic field to electrons, manifested as an increase in electron temperature. Weak or no ion coupling was observed in either event. Results from particle-in-cell simulations of magnetic reconnection with and without a strong guide field are qualitatively consistent with observations. Our results imply that magnetic reconnection is another electron acceleration/heating process inside foreshock transients and could play an important role in shock dynamics.

1. Introduction

Magnetic reconnection, a fundamental energy conversion process in plasmas, was recently found to be associated with collisionless shock environments. In the turbulent magnetosheath downstream of the bow shock, Phan et al. (2018) identified electron magnetic reconnection without ion coupling. They showed observations of an electron-scale current sheet with bidirectional super-ion-Alfvénic electron jets, parallel electric field, and energy conversion from electromagnetic field to particles. Their results suggest the potential role of energy dissipation in turbulent plasmas at the electron scale. Within the shock transition region, magnetic reconnection was also observed, implying its contribution to shock dissipation (Gingell et al., 2019; Wang et al., 2019). Particle-in-cell and hybrid simulations also demonstrated magnetic reconnection at shocks (Bessho et al., 2019; Gingell et al., 2017; Matsumoto et al., 2015).

Because of shock-accelerated particles traveling upstream of quasi-parallel shocks, a foreshock region develops there (e.g., Eastwood et al., 2005). The foreshock is very dynamic and associated with many types of ion-kinetic structures collectively referred to as foreshock transients. These structures are characterized by significant perturbations in field strength and plasma parameters (e.g., Eastwood et al., 2005). Hot flow anomalies (HFAs) (e.g., Omidi & Sibeck, 2007; Schwartz et al., 1985; Zhang et al., 2010) and foreshock bubbles are two most distinct foreshock transients (e.g., Liu et al., 2015; Omidi et al., 2010; Turner et al., 2013). They form when a solar wind discontinuity concentrates and thermalizes foreshock ions causing localized high thermal pressure. Such high thermal pressure pushes the surrounding plasma resulting in a hot, tenuous core bounded by compressional boundaries. The magnetic field inside the core is typically very turbulent. A flux rope was observed inside an HFA (Bai et al., 2020; Hasegawa et al., 2012), which suggests the possibility that magnetic reconnection could occur inside foreshock transients just like in the magnetosheath, bow shock transition region, magnetopause, and plasma sheet and provide

particle acceleration/heating (e.g., Burch & Phan, 2016; Eriksson et al., 2016; Phan et al., 2018; Torbert et al., 2018).

Particle acceleration/heating, almost always observed inside foreshock transients (Liu et al., 2017), could be very important in the shock acceleration process, including providing a seed population for further acceleration, thus increasing the shock acceleration efficiency (e.g., Liu et al., 2016; Liu et al., 2019; Turner et al., 2018; Wilson et al., 2016). Fermi acceleration (Liu et al., 2017; Liu et al., 2018; Turner et al., 2018) and betatron acceleration (Liu et al., 2019) have been identified as two important acceleration mechanisms inside foreshock transients, but more mechanisms, yet to be revealed, might also be implicated. Magnetic reconnection may be such a mechanism. Here, we reveal observational evidence for this process and confirm its presence by comparison with particle-in-cell simulations.

2. Data and Methods

We used data from the National Aeronautics and Space Administration's (NASA) Magnetospheric Multiscale mission (MMS; Burch et al., 2016). We analyzed plasma data from the Fast Plasma Investigation instrument (Pollock et al., 2016), DC magnetic field data from the fluxgate magnetometer (Russell et al., 2016), magnetic field wave data from the search coil magnetometer (Le Contel et al., 2016), and electric field data from axial and spin-plane double-probe electric-field sensors (Ergun et al., 2016; Lindqvist et al., 2016).

We use a two-dimensional particle-in-cell simulation model in which electrons and ions are all treated as full particles and advanced in time by solving the equation of motion. Electric field and magnetic field are defined on grids and updated in time by solving Maxwell's equations using an explicit algorithm. The simulation domain is a two-dimensional box in the x - z plane, $[0, L_x] \times [-L_z/2, L_z/2]$. The initial configuration is the Harris current sheet with the magnetic field $\mathbf{B} = B_0 \tanh(z/L) \mathbf{e}_x + B_{y0} \mathbf{e}_y$, and the plasma density $n = n_b + n_0 \text{sech}^2(z/L)$. Here, B_0 is the asymptotical magnitude of the magnetic field, L is the half-width of the current sheet, B_{y0} is the uniform guide field in the y direction (out-of-plane direction), n_0 is the peak density of the Harris current sheet, and n_b is the background density. Two cases with different values of guide field B_{y0} are considered to compare with the two MMS events. Case 1 has a strong guide field, $B_{y0} = 1.0B_0$; Case 2 has a weak guide field, $B_{y0} = 0.1B_0$. In these two cases, the background density is $n_b = 0.2n_0$, and the half-width is $L = 0.5d_i$, where $d_i = c/\omega_{pi}$ is the ion inertial length defined by n_0 . The ion-to-electron temperature is $T_i/T_e = 4$, the ion-to-electron mass ratio is $m_i/m_e = 100$, and the speed of light is $c = 20V_A$, where V_A is the Alfvén speed evaluated using B_0 and n_0 . The grid size is $\Delta x = \Delta z = 0.05d_i$, and the time step is $\Delta t = 0.001 \Omega_{i0}^{-1}$, where $\Omega_{i0} = eB_0/m_i$ is the unit ion gyrofrequency. The size of the simulation domain is $L_x = 102.4d_i$ and $L_z = 25.6d_i$, with grid numbers $N_x = 2048$ and $N_z = 512$. More than 10^8 particles per species are used in each simulation run. Periodic boundary conditions are adopted in the x direction, and perfect conductor boundary conditions are used in the z direction.

3. Observations

Using MMS observations during 2017–2019, we examined around 130 foreshock transients to look for sub-ion scale current sheets associated with demagnetized electrons. We found at least five events that were very likely reconnecting. Here, we present two representative magnetic reconnection events with and without a strong guide field, respectively. The other three events can be found in the supporting information.

3.1. Event 1 With a Strong Guide Field

MMS at the flank of the bow shock ($[6.5, 20.5, 6.4] R_E$ in GSE) observed a large foreshock transient on 10 November 2017 (Figure 1). It had a core with low field strength (Figure 1a), low density (Figure 1b), and strong plasma flow deflection (Figure 1c). The ions were very diffuse (Figure 1d), and the electron energy was enhanced over time (Figure 1e) possibly due to Fermi acceleration (Liu, Lu, et al., 2017). Its estimated spatial structure is sketched in Figure 1f (using methods described in Liu et al. (2016) and Schwartz et al. (2018)). The magnetic field inside the core was very turbulent, suggesting that magnetic reconnection might occur similar to that in the turbulent magnetosheath (Phan et al., 2018). We zoom in to a very small current sheet near the boundary of the core at $\sim 17:26:18$ UT (vertical gray shaded region that is as thin as a line in Figure 1) to apply further analysis.

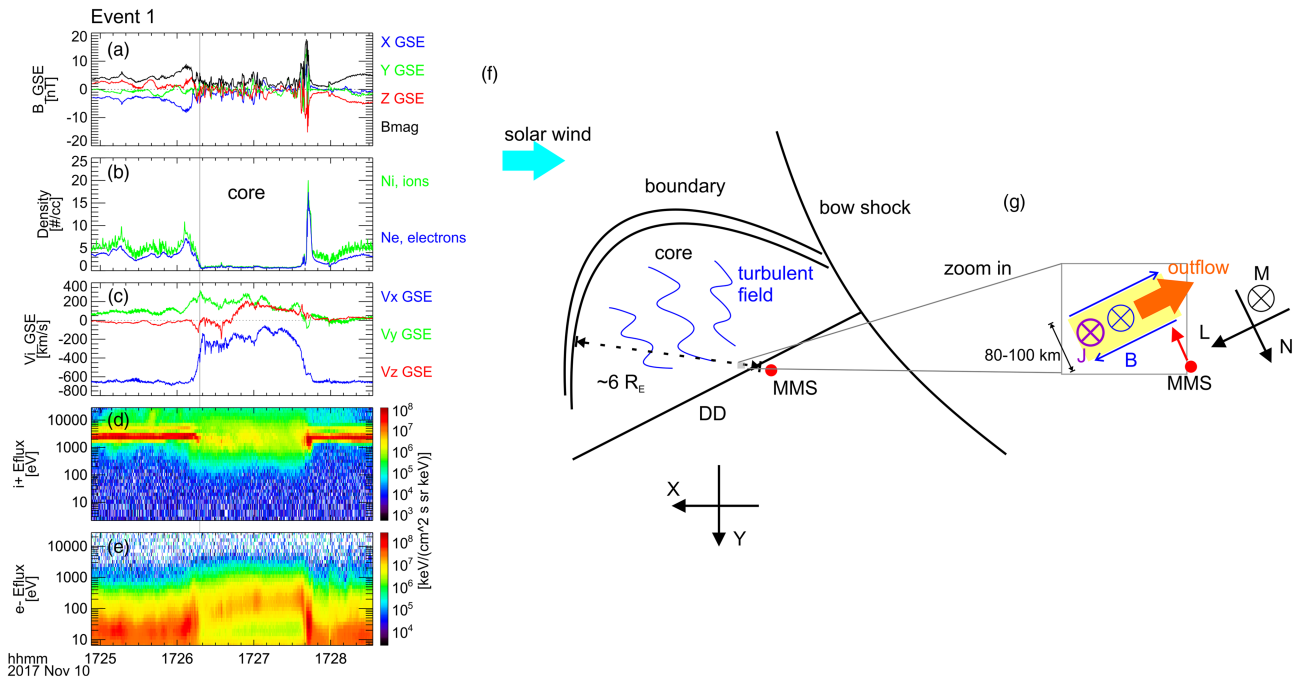


Figure 1. The overview observations of event 1 and its sketch. Panels (a)–(e) are magnetic field in GSE coordinates, plasma density, ion bulk velocity in GSE coordinates, ion energy flux spectrum, and electron energy spectrum, respectively. Panel (f) is the sketch of the foreshock transient geometry in the GSE-XY plane. DD is short for directional discontinuity. Panel (g) is the zoom-in sketch corresponding to the thin gray shaded region in the left panel.

Figure 2 shows the zoom-in plot of the gray shaded region in Figure 1 measured by MMS1 (also see the zoom-in sketch in Figure 1g). By applying minimum variance analysis (Sonnerup & Scheible, 1998) on the magnetic field during the time interval from $\sim 17:26:17.7$ to $17:26:17.9$ UT (Figure 2a, magenta bar at the top), we transformed the GSE to LMN coordinates corresponding to the maximum ($\mathbf{L} = [0.58, 0.24, 0.78]$), intermediate ($\mathbf{M} = [0.64, 0.45, -0.62]$), and minimum ($\mathbf{N} = [-0.50, 0.85, 0.11]$) variance direction, respectively (e.g., Wang et al., 2018). The magnetic field (Figure 2a) exhibited bipolar B_L from about $+2$ to -3 nT, unipolar B_M with maximum value nearly 6 nT, and B_N that was around zero. This indicates that there was very likely a current sheet with a strong guide field (yellow region). The background ion and electron bulk velocity (Figures 2b and 2c) were dominated in the $+N$ direction at ~ 400 – 500 km/s (note that due to the narrow solar wind beam and the presence of foreshock ions, the ion bulk velocity measurement has large uncertainty). We thus estimated the thickness of the current sheet as approximately 80–100 km, which was less than one ion inertial length (~ 218 km before the current sheet and ~ 196 km after the current sheet).

Inside the current sheet (yellow region), the electron bulk velocity V_L was enhanced from -87 ± 66 km/s up to -465 km/s and V_M was enhanced from -106 ± 75 km/s up to -940 km/s, respectively (Figure 2c). The ion bulk velocity was only perturbed by ~ 40 km/s in the L and M directions (Figure 2b), and ion distributions do not show clear variations (Figure S1). Figure 2d shows the current density calculated from the curlometer method (Robert et al., 1998; the interspacecraft separation was ~ 20 km, smaller than the current sheet thickness). There was a strong current density of ~ 130 nA/m² in the $+M$ direction which reversed B_L . Such a magnitude was consistent with the one estimated from the electron and ion bulk velocity difference (~ 800 km/s) and the local density (1.1 cm⁻³ in Figure 2j), which was ~ 140 nA/m². This suggests that the strong current density in the $+M$ direction was mainly carried by electrons. To compare with the measured electron velocity, Figure 2e shows the calculated $\mathbf{E} \times \mathbf{B}$ drift velocity in comparison with ion (dotted) and electron (dashed) perpendicular velocity. Inside the current sheet, electron perpendicular velocity roughly matches $\mathbf{E} \times \mathbf{B}$ drift velocity. Therefore, this current sheet was mainly driven by the electron velocity antiparallel to the guide field.

To examine whether this current sheet was reconnecting, we calculated $\mathbf{j} \cdot \mathbf{E}'$ where $\mathbf{E}' = \mathbf{E} + \mathbf{V}_e \times \mathbf{B}$, the electric field in the electron rest frame. Figure 2g shows that the electric field component parallel to the magnetic

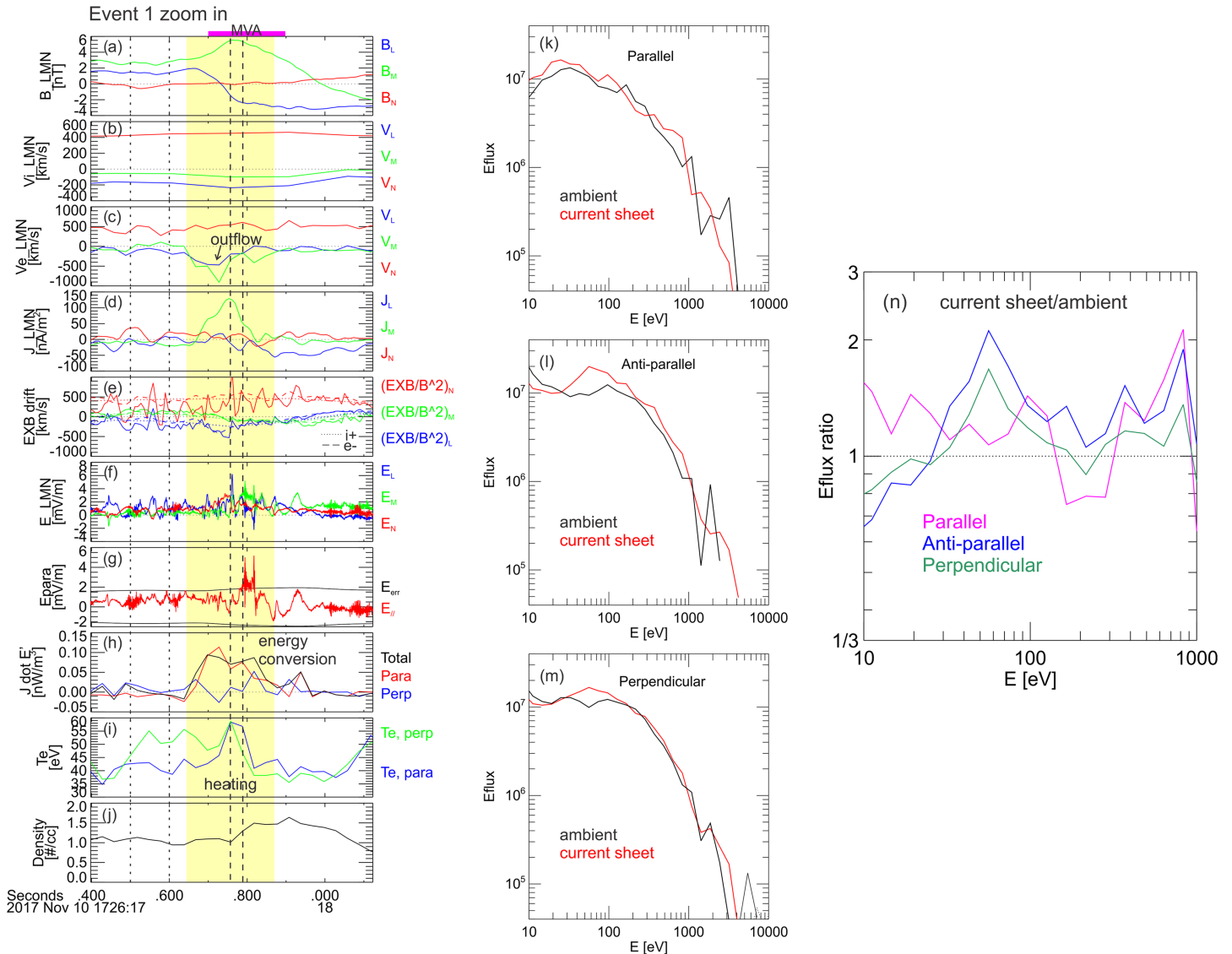


Figure 2. The zoom-in plot of the gray shaded region in Figure 1 measured by MMS1. The left panel from top to bottom are (a) magnetic field in LMN (see definition in the text); (b) ion bulk velocity in LMN; (c) electron bulk velocity in LMN; (d) current density in LMN; (e) $E \times B$ drift velocity in LMN in comparison with ion (dotted) and electron (dashed) perpendicular velocity; (f) electric field in LMN; (g) electric field component parallel to the magnetic field (red) and its error (black); (h) $\mathbf{j} \cdot \mathbf{E}'$ (black), $\mathbf{j}_{\parallel} \cdot \mathbf{E}'_{\parallel}$ (red), and $\mathbf{j}_{\perp} \cdot \mathbf{E}'_{\perp}$ (blue); (i) electron temperature in the parallel (blue) and perpendicular (green) direction; and (j) plasma density. The yellow region indicates the current sheet. Panels (k)–(m) show the electron energy flux spectra inside the current sheet (red; between two vertical dashed lines in the left panel) and in the background (black; between two vertical dotted lines in the left panel), in the direction parallel (k), antiparallel (l), and perpendicular (m) to the magnetic field. Panel (n) shows the ratio between these two energy flux spectra in the parallel (magenta), antiparallel (blue), and perpendicular (green) direction.

field was enhanced inside the current sheet at $\sim 17:26:17.8$ UT (slightly larger than the measurement error). As a result, $\mathbf{j} \cdot \mathbf{E}'$ increased from 0 to ~ 0.12 nW/m³ inside the current sheet, which was dominated by $\mathbf{j}_{\parallel} \cdot \mathbf{E}'_{\parallel}$ (red in Figure 2h). This indicates that the energy was transferred from the field to particles. Indeed, Figure 2i shows that the electron temperature increased inside the current sheet especially in the parallel direction (blue).

To further investigate the electron heating, we plot the time-averaged electron energy flux spectra in the background (between two vertical dotted lines) and in the current sheet (between two vertical dashed lines), respectively. Figures 2k to 2m show their comparison in the direction parallel, antiparallel, and perpendicular to the magnetic field, respectively. We see that in the parallel (Figure 2k) and perpendicular (Figure 2m)

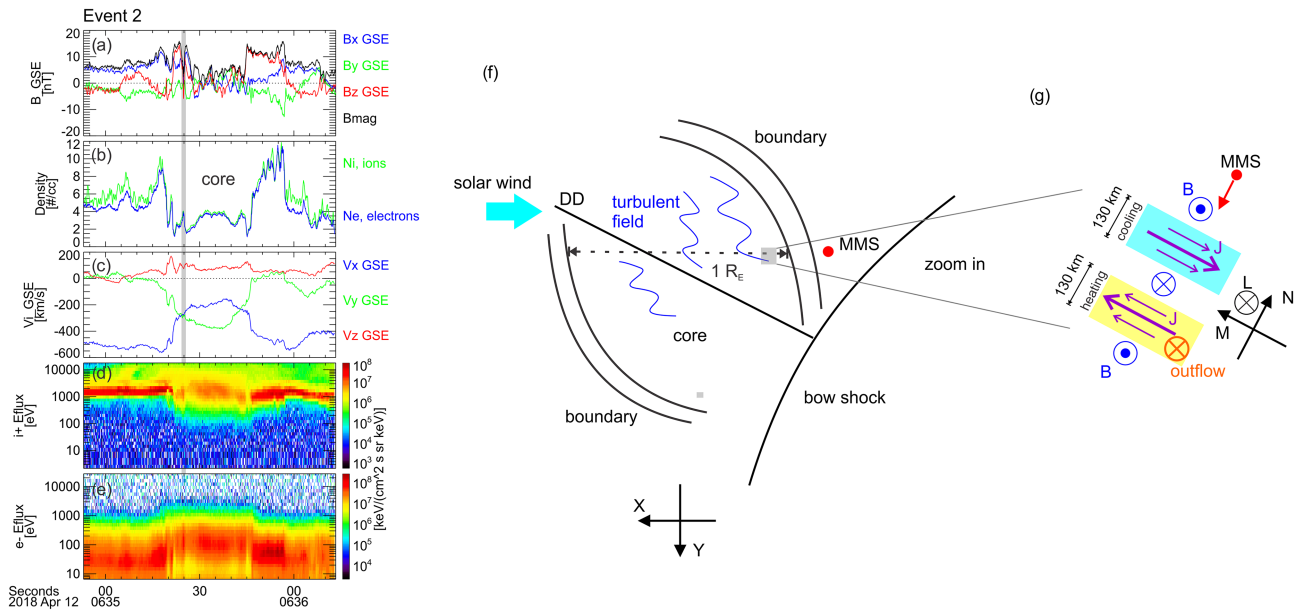


Figure 3. The overview plot and the sketch of Event 2. Same format as in Figure 1.

directions, the energy flux in the current sheet (red) enhanced at tens of eV but did not show clear enhancement above 150 eV compared to the background (black) (also see their energy flux ratios in Figure 2n). In the antiparallel direction (Figure 2l), on the other hand, the energy flux increased by a factor of 1.4 on average (blue in Figure 2n; the uncertainty of energy flux measurement is a few percent) from ~30 eV to 1 keV where the energy flux reached the noise level. Such electron heating/acceleration predominantly in the antiparallel direction is likely because the reconnection electric field was parallel to the guide field consistent with previous simulations (e.g., Huang et al., 2010; Pritchett, 2006). Therefore, this current sheet was reconnecting, transferring energy from the field to electrons mainly in the antiparallel direction. The electron V_L enhancement was thus identified as the electron outflow at ~378 km/s, which was six times the ion Alfvén speed (~63 km/s before the current sheet and ~66 km/s after the current sheet).

3.2. Event 2 Without a Strong Guide Field

MMS at the flank of the bow shock ([6.7, -13.4, 4.6] R_E in GSE) observed another foreshock transient on 12 April 2018 (Figure 3). It also had a core with low field strength (Figure 3a), low density (Figure 3b), and strong plasma flow deflection (Figure 3c) surrounded by two compressional boundaries. There were also diffuse ions (Figure 3d) and electron energy flux enhancement (Figure 3e) inside the core. Figure 3f shows its sketch. Close to the boundary of the core at ~06:35:25 UT (vertical gray shaded region in Figure 3), the local magnetic field dropped to nearly zero, suggesting that there might be magnetic reconnection.

Figure 4 is the zoom-in plot of the shaded region in Figure 3 measured by MMS1 (also see the zoom-in sketch in Figure 3g). We also transformed the GSE to LMN coordinates ($L = [-0.36, -0.22, -0.91]$, $M = [0.83, -0.51, -0.21]$, and $N = [-0.41, -0.83, 0.37]$) using the time interval from ~06:35:24.9 to 06:35:25.3 UT (magenta bar at the top). We see that there were two current sheets (labeled as blue and yellow region, respectively): B_L varied from about -9 to +6 nT and back to -10 nT. Neither of the current sheets had a strong guide field (B_M ranged approximately from -3 to -1 nT). The ion bulk velocity did not show clear variation during the entire time interval (also see ion distributions in Figure S2) and was mainly in the +N direction at ~400 km/s (Figure 4b). Thus, the crossing of two current sheets cannot be an apparent double crossing of a single current sheet moving back and forth. We estimated the thickness of two current sheets to be around 130 km, comparable to one ion inertial length (133 km before two current sheets or 160 km after two current sheets). As for the electron bulk velocity (Figure 4c), moderate variation was observed in the first current sheet (CS 1, blue region) resulting in an electron current mainly in the -M

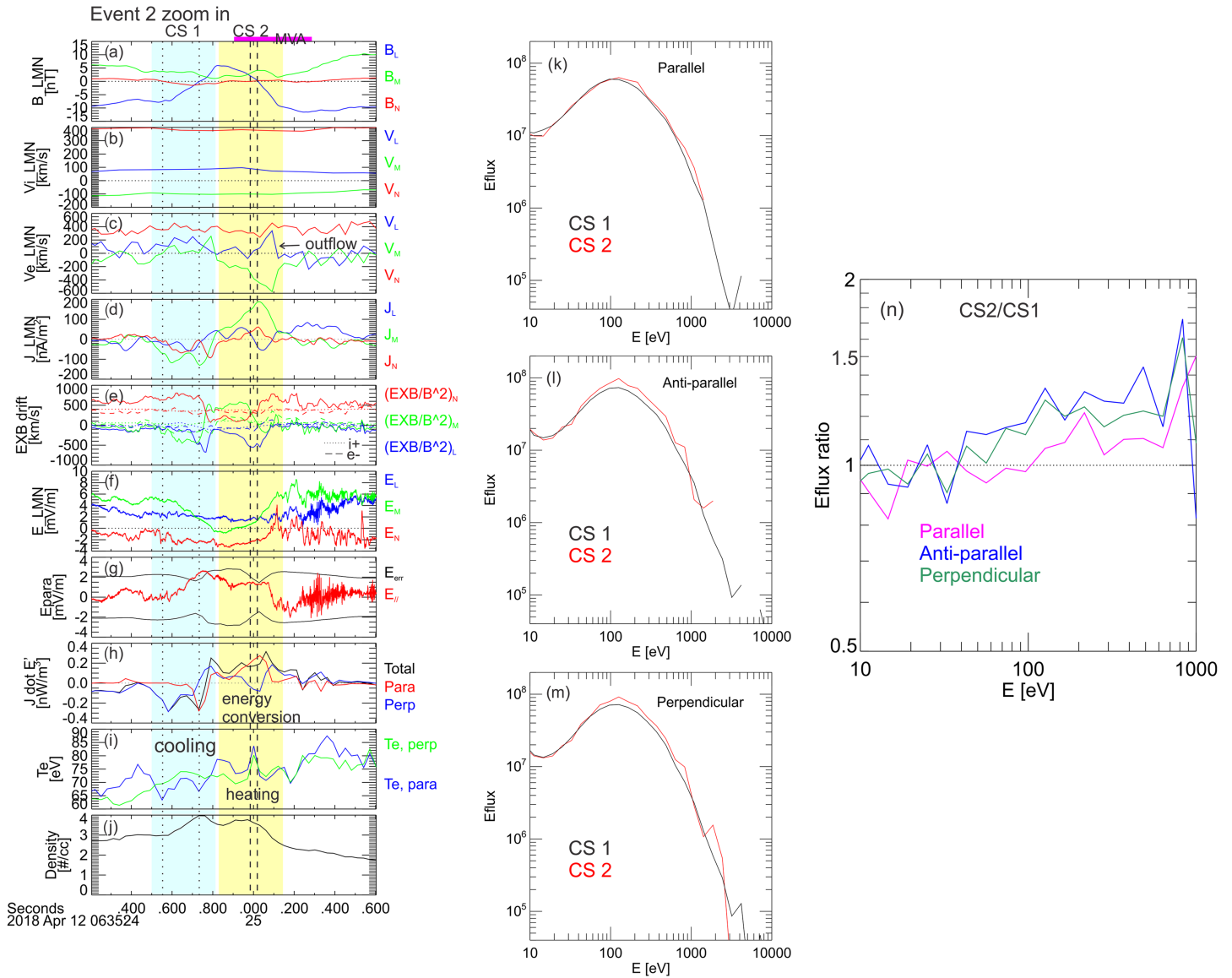


Figure 4. The zoom-in plot of the gray shaded region in Figure 3 measured by MMS1. Same format as in Figure 2, except that the electron energy flux spectra comparison is between two current sheets (between two vertical dotted lines and dashed lines, respectively).

direction at $\sim 100 \text{ nA/m}^2$ (Figure 4d). In the second current sheet (CS 2), the variation was more significant: V_L varied from $-9 \pm 119 \text{ km/s}$ in the background up to 331 km/s and V_M varied from -58 ± 79 up to -570 km/s . The current density was $\sim 190 \text{ nA/m}^2$ mainly in the $+M$ direction, which was more intense than that of CS 1 (Figure 4d). Its magnitude was comparable to that estimated from electron V_M variation ($\sim 230 \text{ nA/m}^2$). Figure 4e shows the $\mathbf{E} \times \mathbf{B}$ drift velocity. We see that it did not match well with electron perpendicular velocity in two current sheets, suggesting that electrons there were (at least partially) demagnetized.

To investigate whether two current sheets were reconnecting, we calculated $\mathbf{j} \cdot \mathbf{E}'$. We see that inside both current sheets, there was enhanced parallel electric field (slightly larger or comparable to the measurement error) and nonzero $\mathbf{j} \cdot \mathbf{E}'$ indicating energy conversion (Figures 4g and 4h). In CS 1, $\mathbf{j} \cdot \mathbf{E}'$ was negative, meaning that the energy was transferred from particles to the field, whereas in CS 2, $\mathbf{j} \cdot \mathbf{E}'$ was positive (dominated by $\mathbf{j}_{\parallel} \cdot \mathbf{E}'_{\parallel}$), meaning that the energy was transferred from the field to particles. As a result, the electron temperature decreased in CS 1 and increased in CS 2 (Figure 4i), and the parallel temperature (blue) varied more

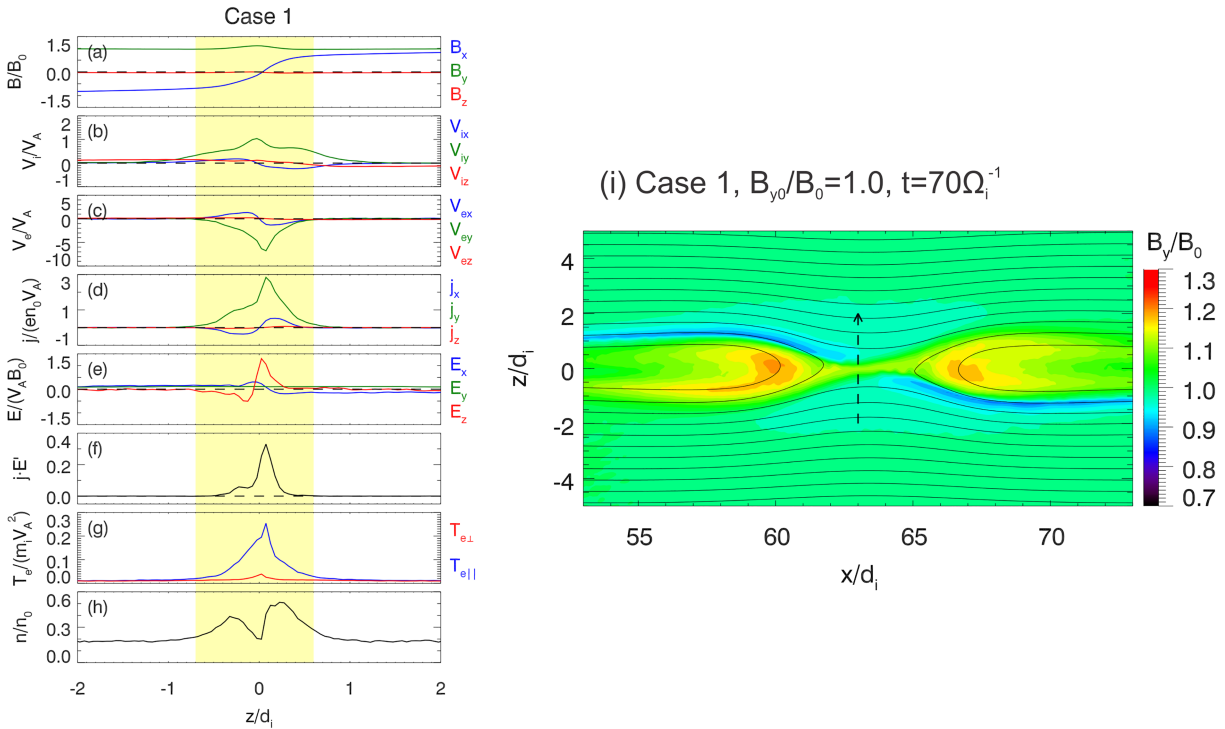


Figure 5. The virtual spacecraft crossing of the simulated electron diffusion region for case 1 with a strong guide field. The left panel from top to bottom are normalized (a) magnetic field, (b) ion bulk velocity, (c) electron bulk velocity, (d) current density, (e) electric field, (f) $\mathbf{j} \cdot \mathbf{E}$, (g) electron temperature, and (h) density. The coordinate system (x , y , and z) is the same as the observations (L, M, and N). The right panel indicates the virtual spacecraft trajectory (dashed arrow) in the xz plane. The black lines indicate the magnetic field lines in the xz plane, and the color indicates the magnitude of B_y .

significantly than the perpendicular temperature (green). (After 06:35:25.2 UT, there was another temperature increase, which was likely corresponding to a different population that was heated/accelerated by the foreshock transient core.) We also compared the energy flux spectra in CS 1 (between two vertical dotted lines) and in CS 2 (between two vertical dashed lines) shown in Figures 4k to 4m. There was no very clear enhancement in the parallel direction (Figure 4k), but in the antiparallel and perpendicular directions, the energy flux in CS 2 enhanced by a factor of 1.3 and 1.2, respectively, compared to that in CS 1 above ~ 100 eV (Figures 4l to 4n). Such energy flux enhancement is consistent with the opposite energy conversion in CS 1 and CS 2. Therefore, we conclude that there was no reconnection inside CS 1 and the electrons were transferring energy to the field. In CS 2, on the other hand, there was reconnection with energy conversion from the field to particles and the associated electron temperature enhancements. The electron V_L enhancement in CS 2 was thus identified as the electron outflow at ~ 340 km/s, faster than the average ion Alfvén speed (115 and 202 km/s in the background before CS 1 and after CS 2, respectively).

4. Simulations

To compare with two observation events, we employed particle-in-cell simulations of two magnetic reconnection cases with and without a strong guide field, respectively. For Case 1, with a strong guide field, the left panel of Figure 5 shows the virtual spacecraft crossing of the electron diffusion region (embedded in the ion diffusion region) along the normal direction, and the right panel shows the virtual spacecraft trajectory. The coordinate system (x , y , and z) is the same as in the observations (L, M, and N). Figure 5a shows that B_y is comparable to B_x , indicating a strong guide field. The thickness of the current sheet is around one ion inertial length, consistent with observations. Within the current sheet (yellow shaded region), the ion velocity perturbation in the x direction is very weak, $\sim 0.2 V_A$ (Figure 5b; note that the value varies across different virtual trajectories, but the order of magnitude is similar), consistent with event 1 ($\sim 0.6 V_A$). The electron outflow, on the other hand, is very clear in both $+x$ and $-x$ directions at $\sim \pm 1.5 V_A$ (Figure 5c; also depending

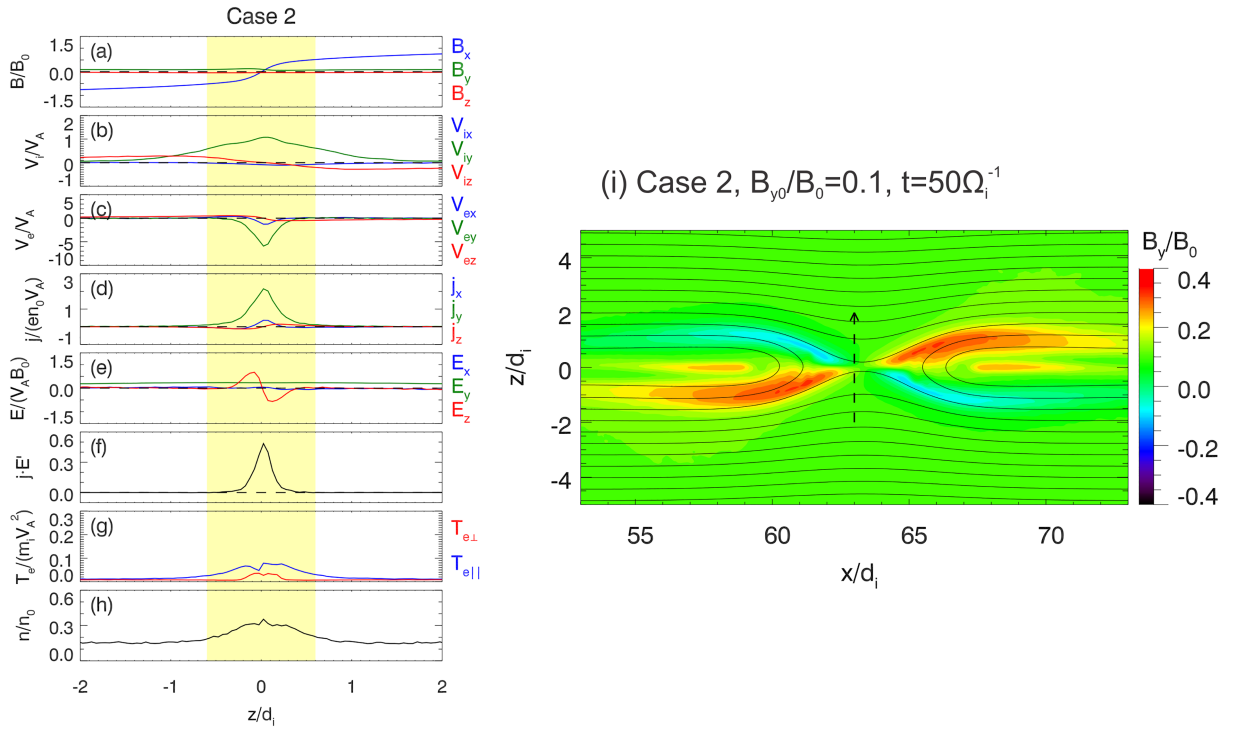


Figure 6. The virtual spacecraft crossing of the simulated electron diffusion region for Case 2 without a strong guide field. Same format as in Figure 5.

on the virtual trajectory). In the y direction, there is moderate ion velocity enhancement at $\sim 1.0 V_A$ (Figure 5b) and significant electron velocity enhancement at approximately $-7.0 V_A$ (Figure 5c), resulting in strong current density in the $+y$ direction (Figure 5d). A positive $\mathbf{j} \cdot \mathbf{E}'$ can be seen (Figure 5f), resulting in electron temperature enhancements (Figure 5g). The parallel temperature increase (blue) is more dominant than the perpendicular temperature increase (green), which is consistent with observations in Event 1 (Figures 2i, 2k to 2n).

Figure 6 shows the virtual spacecraft crossing of the simulated current sheet without a strong guide field (Case 2). The thickness of the current sheet is also around one ion inertial length. Similar to observations in Event 2 (Figures 4b and 4c), no ion outflow is seen (Figure 6b), but there is clear electron outflow in the x direction at approximately $-1.5 V_A$ (Figure 6c). The strong current density in the $+y$ direction (Figure 6d) is also mainly contributed by the electron velocity enhancement in the $-y$ direction (Figure 6c). There is also positive $\mathbf{j} \cdot \mathbf{E}'$ (Figure 6f) resulting in the electron temperature increases (Figure 6g). Similar to observations in Event 2 (Figures 4i, 4k to 4n), the parallel temperature increase (blue) is only slightly larger than the perpendicular temperature increase (green). In summary, the simulation results are qualitatively consistent with our observational results in both events, further confirming that the observed current sheets were reconnecting.

5. Conclusions and Discussion

Using MMS observations, we have provided the first direct observational evidence of magnetic reconnection inside foreshock transients. We showed two events with and without a strong guide field, respectively. In both events, the reconnection occurred in microscale current sheets with thickness less than or comparable to one ion inertial length. We identified a super-ion-Alfvénic electron outflow, positive $\mathbf{j} \cdot \mathbf{E}'$, and the electron temperature increases. Weak or no ion coupling was observed. We also applied particle-in-cell simulations to compare with two observation events, which are qualitatively consistent. Liu, Angelopoulos, et al. (2017) discussed energy conversion processes from kinetic foreshock ions to electromagnetic field to electrons inside foreshock transients—our results show that magnetic reconnection is also one such process.

Thus, we find that magnetic reconnection occurs not only downstream of and inside shocks but also upstream of shocks, contributing to dissipation at the sub-ion scale.

Here, we discuss what might trigger the magnetic reconnection. In two events shown here and three events in the supporting information, reconnecting current sheets were all inside HFAs or foreshock bubbles that are associated with a solar wind discontinuity. Hybrid simulations and observations showed that magnetic reconnection can occur when a solar wind discontinuity is compressed by the bow shock (Hamrin et al., 2019; Lin, 1997). It is likely that the reconnecting current sheet originated in the driver solar wind discontinuity and was compressed by the foreshock transient as two events occurred at the edge of the foreshock transient where the driver discontinuity might be (Figures 1 and S5). Additionally, the rest events were likely inside the hot low-density core with turbulent magnetic field indicating that the reconnecting current sheet may also originate in the turbulent magnetic field, a situation similar to the magnetosheath (Phan et al., 2018). However, although clear ion coupling was not observed, the events may still necessitate ion coupling. Their spatial scale was around one ion inertial length, inconsistent with the typical electron magnetic reconnection scale (several electron inertial lengths; Phan et al., 2018). Therefore, the events could be the electron diffusion region embedded in the ion diffusion region as shown in our simulations. The observational evidence of ion diffusion region needs further study in the future.

Next, we discuss the possible effects of the guide field by comparing observation Event 1 and simulation Case 1 with Event 2 and Case 2. We see that with a strong guide field, the parallel temperature enhancement is more dominant than the perpendicular temperature enhancement (Figures 2i, 2k to 2n, 5g). Without a strong guide field, on the other hand, the parallel temperature enhancement is comparable to the perpendicular temperature enhancement (Figures 4i, 4k to 4n, 6g). This result is consistent with previous simulation studies (e.g., Swisdak et al., 2005). Here, we discuss what might cause such difference in the parallel/perpendicular temperature enhancement. One possible mechanism is that the strong guide field can help confine electrons within the diffusion region through gyration to increase the acceleration time and enhance the parallel heating (Fu et al., 2006). In addition, with a strong guide field, electrons can get preaccelerated by the parallel electric field in the separatrix region before moving into the electron diffusion region (Drake et al., 2005; Pritchett, 2006). Another possibility is that the perpendicular heating is suppressed by the guide field (Phan et al., 2013). However, when and where MMS and the virtual spacecraft crossed the current sheet can also result in apparent differences in two events and cases. To understand the role of the guide field requires more comprehensive studies.

As one of the most important acceleration mechanisms in the universe, shock acceleration is still not fully understood. For example, there is a minimum energy threshold for particles to participate in the shock acceleration process, but the source of the initial energization is unknown (i.e., the “injection problem”; Treumann, 2009 and references therein). Supercritical shocks can intrinsically reflect particles forming the foreshock with many large-scale ion kinetic foreshock transients. Magnetic reconnection inside foreshock transients could provide additional acceleration/heating increasing the theoretical acceleration efficiency of shocks and contributing to the initial energization of particles upstream of shocks.

Acknowledgments

We acknowledge the International Space Science Institute for providing a collaborative opportunity for this work. Work at UCLA is supported by National Aeronautics and Space Administration (NASA) contract NNX08AO83G. T. Z. L. is supported by the NASA Living With a Star Jack Eddy Postdoctoral Fellowship Program, administered by the Cooperative Programs for the Advancement of Earth System Science. T. Z. L. and S. L. are partially supported by National Science Foundation (NSF) award AGS-1941012. H. Z. is partially supported by NSF AGS-1352669 and NASA contract 80NSSC18K1376. MMS data are available at MMS Science Data Center (<https://lasp.colorado.edu/mms/sdc/>). We thank the SPEDAS software team and NASA's Coordinated Data Analysis Web (CDAWeb, <http://cdaweb.gsfc.nasa.gov/>) for their analysis tools and data access. The SPEDAS software (see Angelopoulos et al. (2019) is available at <http://themis.ssl.berkeley.edu>).

References

- Angelopoulos, V., Cruce, P., Drozdov, A., Grimes, E. W., Hatzigeorgiu, N., King, D. A., et al. (2019). The Space Physics Environment Data Analysis System (SPEDAS). *Space Science Reviews*, 215(1), 9. <https://doi.org/10.1007/s11214-018-0576-4>
- Bai, S.-C., Shi, Q., Liu, T. Z., Zhang, H., Yue, C., Sun, W.-J., et al. (2020). Ion-scale flux rope observed inside a hot flow anomaly. *Geophysical Research Letters*, 47, e2019GL085933. <https://doi.org/10.1029/2019GL085933>
- Bessho, N., Chen, L.-J., Wang, S., Hesse, M., & Wilson, L. B. (2019). Magnetic reconnection in a quasi-parallel shock: Two-dimensional local particle-in-cell simulation. *Geophysical Research Letters*, 46, 9352–9361. <https://doi.org/10.1029/2019GL083397>
- Burch, J. L., Moore, T. E., Torbert, R. B., & Giles, B. L. (2016). Magnetospheric Multiscale overview and science objectives. *Space Science Reviews*, 199(1–4), 5–21. <https://doi.org/10.1007/s11214-015-0164-9>
- Burch, J. L., & Phan, T. D. (2016). Magnetic reconnection at the dayside magnetopause: Advances with MMS. *Geophysical Research Letters*, 43, 8327–8338. <https://doi.org/10.1002/2016GL069787>
- Drake, J. F., Shay, M. A., Thongthai, W., & Swisdak, R. A. (2005). Production of energetic electrons during magnetic reconnection. *Physical Review Letters*, 94(9), 095001. <http://doi.org/10.1103/PhysRevLett.94.095001>
- Eastwood, J. P., Lucek, E. A., Mazelle, C., Meziane, K., Narita, Y., Pickett, J., & Treumann, R. A. (2005). The foreshock. *Space Science Reviews*, 118, 41–94. <https://doi.org/10.1007/s11214-005-3824-3>
- Ergun, R. E., Tucker, S., Westfall, J., Goodrich, K. A., Malaspina, D. M., Summers, D., et al. (2016). The axial double probe and fields signal processing for the MMS mission. *Space Science Reviews*, 199(1–4), 167–188. <https://doi.org/10.1007/s11214-014-0115-x>

- Eriksson, S., Lavraud, B., Wilder, F. D., Stawarz, J. E., Giles, B. L., Burch, J. L., et al. (2016). Magnetospheric Multiscale observations of magnetic reconnection associated with Kelvin-Helmholtz waves. *Geophysical Research Letters*, *43*, 5606–5615. <https://doi.org/10.1002/2016GL068783>
- Fu, X. R., Lu, Q. M., & Wang, S. (2006). The process of electron acceleration during collisionless magnetic reconnection. *Physics of Plasmas*, *13*, 012309. <https://doi.org/10.1063/1.2164808>
- Gingell, I., Schwartz, S. J., Burgess, D., Johlander, A., Russell, C. T., Burch, J. L., et al. (2017). MMS observations and hybrid simulations of surface ripples at a marginally quasi-parallel shock. *Journal of Geophysical Research: Space Physics*, *122*, 11,003–11,017. <https://doi.org/10.1002/2017JA024538>
- Gingell, I., Schwartz, S. J., Eastwood, J. P., Burch, J. L., Ergun, R. E., Fuselier, S., et al. (2019). Observations of magnetic reconnection in the transition region of quasi-parallel shocks. *Geophysical Research Letters*, *46*, 1177–1184. <https://doi.org/10.1029/2018GL081804>
- Hamrin, M., Gunell, H., Goncharov, O., de Spiegeleer, A., Fuselier, S., Mukherjee, J., et al. (2019). Can reconnection be triggered as a solar wind directional discontinuity crosses the bow shock?—A case of asymmetric reconnection. *Journal of Geophysical Research: Space Physics*, *124*, 8507–8523. <https://doi.org/10.1029/2019JA027006>
- Hasegawa, H., Zhang, H., Lin, Y., Sonnerup, B. U. Ö., Schwartz, S. J., Lavraud, B., & Zong, Q.-G. (2012). Magnetic flux rope formation within a magnetosheath hot flow anomaly. *Journal of Geophysical Research*, *117*, A09214. <https://doi.org/10.1029/2012JA017920>
- Huang, C., Lu, Q., & Wang, S. (2010). The mechanisms of electron acceleration in antiparallel and guide field magnetic reconnection. *Physics of Plasmas*, *17*, 072306. <https://doi.org/10.1063/1.3457930>
- le Contel, O., Leroy, P., Roux, A., Coillot, C., Alison, D., Bouabdellah, A., et al. (2016). The search-coil magnetometer for MMS. *Space Science Reviews*, *199*(1–4), 257–282. <https://doi.org/10.1007/s11214-014-0096-9>
- Lin, Y. (1997). Generation of anomalous flows near the bow shock by its interaction with interplanetary discontinuities. *Journal of Geophysical Research*, *102*(A11), 24,265–24,281. <https://doi.org/10.1029/97JA01989>
- Lindqvist, P.-A., Olsson, G., Torbert, R. B., King, B., Granoff, M., Rau, D., et al. (2016). The spin-plane double probe electric field instrument for MMS. *Space Science Reviews*, *199*(1–4), 137–165. <https://doi.org/10.1007/s11214-014-0116-9>
- Liu, T. Z., Angelopoulos, V., Hietala, H., & Wilson, L. B. III (2017). Statistical study of particle acceleration in the core of foreshock transients. *Journal of Geophysical Research: Space Physics*, *122*, 7197–7208. <https://doi.org/10.1002/2017JA024043>
- Liu, T. Z., Angelopoulos, V., & Lu, S. (2019). Relativistic electrons generated at Earth's quasi-parallel bow shock. *Science Advances*, *5*, 7. <https://doi.org/10.1126/sciadv.aaw1368>
- Liu, T. Z., Hietala, H., Angelopoulos, V., & Turner, D. L. (2016). Observations of a new foreshock region upstream of a foreshock bubble's shock. *Geophysical Research Letters*, *43*, 4708–4715. <https://doi.org/10.1002/2016GL068984>
- Liu, T. Z., Lu, S., Angelopoulos, V., Hietala, H., & Wilson, L. B. III (2017). Fermi acceleration of electrons inside foreshock transient cores. *Journal of Geophysical Research: Space Physics*, *122*, 9248–9263. <https://doi.org/10.1002/2017JA024480>
- Liu, T. Z., Lu, S., Angelopoulos, V., Lin, Y., & Wang, X. Y. (2018). Ion acceleration inside foreshock transients. *Journal of Geophysical Research: Space Physics*, *123*, 163–178. <https://doi.org/10.1002/2017JA024838>
- Liu, T. Z., Turner, D. L., Angelopoulos, V., & Omid, N. (2016). Multipoint observations of the structure and evolution of foreshock bubbles and their relation to hot flow anomalies. *Journal of Geophysical Research: Space Physics*, *121*, 5489–5509. <https://doi.org/10.1002/2016JA022461>
- Liu, Z., Turner, D. L., Angelopoulos, V., & Omid, N. (2015). THEMIS observations of tangential discontinuity-driven foreshock bubbles. *Geophysical Research Letters*, *42*, 7860–7866. <https://doi.org/10.1002/2015GL065842>
- Matsumoto, Y., Amano, T., Kato, N. T., & Hoshino, M. (2015). Stochastic electron acceleration during spontaneous turbulent reconnection in a strong shock wave. *Science*, *347*(6225), 974–978. <https://doi.org/10.1126/science.1260168>
- Omid, N., Eastwood, J. P., & Sibeck, D. G. (2010). Foreshock bubbles and their global magnetospheric impacts. *Journal of Geophysical Research*, *115*, A06204. <https://doi.org/10.1029/2009JA014828>
- Omid, N., & Sibeck, D. G. (2007). Formation of hot flow anomalies and solitary shocks. *Journal of Geophysical Research*, *112*, A10203. <https://doi.org/10.1029/2006JA011663>
- Phan, T. D., Eastwood, J. P., Shay, M. A., Drake, J. F., Sonnerup, B. U. Ö., Fujimoto, M., et al. (2018). Electron magnetic reconnection without ion coupling in Earth's turbulent magnetosheath. *Nature*, *557*(7704), 202–206. <https://doi.org/10.1038/s41586-018-0091-5>
- Phan, T. D., Shay, M. A., Gosling, J. T., Fujimoto, M., Drake, J. F., Paschmann, G., et al. (2013). Electron bulk heating in magnetic reconnection at Earth's magnetopause: Dependence on the inflow Alfvén speed and magnetic shear. *Geophysical Research Letters*, *40*, 4475–4480. <https://doi.org/10.1002/grl.50917>
- Pollock, C., Moore, T., Jacques, A., Burch, J., Gliese, U., Saito, Y., et al. (2016). Fast plasma investigation for Magnetospheric Multiscale. *Space Science Reviews*, *199*(1–4), 331–406. <https://doi.org/10.1007/s11214-016-0245-4>
- Pritchett, P. L. (2006). Relativistic electron production during guide field magnetic reconnection. *Journal of Geophysical Research*, *111*, A10212. <http://doi.org/10.1029/2006JA011793>
- Robert, P., Dunlop, M. W., Roux, A., & Chanteur, G. (1998). Accuracy of current density determination. *ISSI Scientific Reports Series*, *1*, 395–418.
- Russell, C. T., Anderson, B. J., Baumjohann, W., Bromund, K. R., Dearborn, D., Fischer, D., et al. (2016). The Magnetospheric Multiscale magnetometers. *Space Science Reviews*, *199*(1–4), 189–256. <https://doi.org/10.1007/s11214-014-0057-3>
- Schwartz, S. J., Avakov, L., Turner, D., Zhang, H., Gingell, I., Eastwood, J. P., et al. (2018). Ion kinetics in a hot flow anomaly: MMS observations. *Geophysical Research Letters*, *45*, 11,520–11,529. <https://doi.org/10.1029/2018GL080189>
- Schwartz, S. J., Chaloner, C. P., Christiansen, P. J., Coates, A. J., Hall, D. S., Johnstone, A. D., et al. (1985). An active current sheet in the solar wind. *Nature*, *318*(6043), 269–271. <https://doi.org/10.1038/318269a0>
- Sonnerup, B. U. Ö., & Scheible, M. (1998). Minimum and maximum variance analysis. In G. Paschmann, & P. W. Daly (Eds.), *Analysis methods for multi spacecraft data*, (pp. 185–215). Bern, Switzerland: European Space Agency.
- Swisdak, M., Drake, J. F., Shay, M. A., & McIlhargey, J. G. (2005). Transition from antiparallel to component magnetic reconnection. *Journal of Geophysical Research*, *110*, A05210. <https://doi.org/10.1029/2004JA010748>
- Torbert, R. B., Burch, J. L., Phan, T. D., Hesse, M., Argall, M. R., Shuster, J., et al. (2018). Electron-scale dynamics of the diffusion region during symmetric magnetic reconnection in space. *Science*, *362*(6421), 1391–1395. <https://doi.org/10.1126/science.aat2998>
- Treumann, R. A. (2009). Fundamentals of collisionless shocks for astrophysical application, 1. Non-relativistic shocks. *Astron. Astrophysics Review*, *17*, 409.
- Turner, D. L., Omid, N., Sibeck, D. G., & Angelopoulos, V. (2013). First observations of foreshock bubbles upstream of Earth's bow shock: Characteristics and comparisons to HFAs. *Journal of Geophysical Research: Space Physics*, *118*, 1552–1570. <https://doi.org/10.1002/jgra.50198>

- Turner, D. L., Wilson LB 3rd, Liu, T. Z., Cohen, I. J., Schwartz, S. J., Osmane, A., et al. (2018). Autogenous and efficient acceleration of energetic ions upstream of Earth's bow shock. *Nature*, *561*(7722), 206–210. <https://doi.org/10.1038/s41586-018-0472-9>
- Wang, R., Lu, Q., Nakamura, R., Baumjohann, W., Huang, C., Russell, C. T., et al. (2018). An electron-scale current sheet without bursty reconnection signatures observed in the near-Earth tail. *Geophysical Research Letters*, *45*, 4542–4549. <https://doi.org/10.1002/2017GL076330>
- Wang, S., Chen, L.-J., Bessho, N., Hesse, M., Wilson, L. B. III, Giles, B., et al. (2019). Observational evidence of magnetic reconnection in the terrestrial bow shock transition region. *Geophysical Research Letters*, *46*, 562–570. <https://doi.org/10.1029/2018GL080944>
- Wilson, L. B. I. I., Sibeck, D. G., Turner, D. L., Osmane, A., Caprioli, D., & Angelopoulos, V. (2016). Relativistic electrons produced by foreshock disturbances observed upstream of Earth's bow shock. *Physical Review Letters*, *117*, 215101. <https://doi.org/10.1103/PhysRevLett.117.215101>
- Zhang, H., Sibeck, D. G., Zong, Q. G., Gary, S. P., McFadden, J. P., Larson, D., et al. (2010). Time history of events and macroscale interactions during substorms observations of a series of hot flow anomaly events. *Journal of Geophysical Research*, *115*, A12235. <https://doi.org/10.1029/2009JA015180>

References from Supporting Information

- Chen, L.-J., Hesse, M., Wang, S., Bessho, N., & Daughton, W. (2016). Electron energization and structure of the diffusion region during asymmetric reconnection. *Geophysical Research Letters*, *43*, 2405–2412. <https://doi.org/10.1002/2016GL068243>
- Hwang, K.-J., Sibeck, D. G., Choi, E., Chen, L. J., Ergun, R. E., Khotyaintsev, Y., et al. (2017). Magnetospheric Multiscale mission observations of the outer electron diffusion region. *Geophysical Research Letters*, *44*, 2049–2059. <https://doi.org/10.1002/2017GL072830>